

DMD # 20545

Comparison of the Bioactivation Potential of the Antidepressant and Hepatotoxin Nefazodone with Aripiprazole, a Structural Analog and Marketed Drug

Jonathan N. Bauman, Kosea S. Frederick, Aarti Sawant, Robert L.
Walsky, Loretta M. Cox, Ronald S. Obach, and Amit S. Kalgutkar

*Pharmacokinetics, Dynamics and Metabolism, Pfizer Global Research and Development,
Groton, Connecticut*

DMD # 20545

Running Title: Comparative Studies on the Metabolism/Bioactivation of Aripiprazole
and Nefazodone

Number of Text Pages: (including references) 28

Number of Tables: 3

Number of Figures: 10

Number of References: 29

Number of Words in Abstract: 251

Number of Words in Introduction: 700

Number of Words in Discussion: 1501

Abbreviations used are: ADR, adverse drug reaction; 2-[3-[4-(3-Chlorophenyl)-1-piperazinyl]propyl-5-ethyl-2,4-dihydro-4-(2-phenoxyethyl)-3*H*-1,2,4-triazol-3-one, nefazodone; 7-[4-[4-(2,3-dichlorophenyl)-1-piperazinyl]butoxy]-3,4-dihydrocarbostyryl, aripiprazole; **1**, *para*-hydroxynefazodone; GSH, reduced glutathione; LC-MS/MS, liquid chromatography tandem mass spectrometry; CID, collision-induced dissociation; MRM-EPI, multiple reaction monitoring-enhanced product ion, R_t , retention time.

Correspondence should be addressed to: Amit S. Kalgutkar, Pharmacokinetics, Dynamics, and Metabolism Department, Pfizer Global Research and Development, Groton, CT 06340. Phone: (860)-715-2433. E-mail: amit.kalgutkar@pfizer.com

DMD # 20545

Abstract

In vitro metabolism/bioactivation of structurally-related CNS agents nefazodone (hepatotoxin) and aripiprazole (non-hepatotoxin) were undertaken in human liver microsomes in an attempt to understand the differences in toxicological profile. NADPH-supplemented microsomal incubations of nefazodone and glutathione generated conjugates derived from addition of thiol to quinonoid intermediates. Inclusion of cyanide afforded cyano conjugates to iminium ions derived from α -carbon oxidation of the piperazine ring in nefazodone and downstream metabolites. While the arylpiperazine motif in aripiprazole did not succumb to bioactivation, the dihydroquinolinone group was bioactivated via an intermediate monohydroxy metabolite to a reactive species, which was trapped by glutathione. Studies with synthetic dehydroaripiprazole metabolite revealed an analogous glutathione conjugate with molecular weight 2 Da lower. Based on the proposed structure of the glutathione conjugate(s), a bioactivation sequence involving aromatic *ortho*- or *para*-hydroxylation on the quinolinone followed by oxidation to a quinone-imine was proposed. P4503A4 inactivation studies in microsomes indicated that unlike nefazodone, aripiprazole was not a time- and concentration-dependent inactivator of the enzyme. Overall, these studies reinforce the notion that not all drugs that are bioactivated in vitro elicit a toxicological response in vivo. A likely explanation for the markedly improved safety profile of aripiprazole (versus nefazodone) despite the accompanying bioactivation liability are the vastly improved pharmacokinetics (enhanced oral bioavailability, longer elimination half-life) due to reduced P4503A4-mediated metabolism/bioactivation, which result in a lower daily dose (5-20 mg/day) compared

DMD # 20545

with nefazodone (200-400 mg/day). This attribute probably reduces the total body burden to reactive metabolite exposure and may not exceed a threshold needed for toxicity.

Introduction

In an increasing number of cases, a broader understanding of the biochemical basis for adverse drug reactions (ADRs) has aided to replace a vague perception of a chemical class effect with a sharper picture of an individual molecular peculiarity. Evidence from such investigations suggests that bioactivation of drugs to reactive intermediates constitutes a rate-limiting step in the etiology of some ADRs (Nelson, 2001; Evans et al., 2004; Park et al., 2005; Kalgutkar et al., 2005a; Kalgutkar and Soglia, 2005). Information to qualify certain functional groups as “structural alerts” or “toxicophores” also has been inferred from such studies based on myriad examples of protoxins containing these motifs, which are bioactivated to reactive metabolites (Kalgutkar et al., 2005a).

Consequently, there often exists a notion among medicinal chemists that structural alerts should be generally avoided in drug design efforts. Such a strategy has also come under scrutiny given the plethora of examples of drugs devoid of ADRs despite containing toxicophores susceptible to bioactivation. An interesting example of this dilemma is evident with the CNS agents 2-[3-[4-(3-chlorophenyl)-1-piperazinyl]propyl-5-ethyl-2,4-dihydro-4-(2-phenoxyethyl)-3*H*-1,2,4-triazol-3-one (nefazodone) and 7-[4-[4-(2,3-dichlorophenyl)-1-piperazinyl]butoxy]-3,4-dihydrocarbostyryl (aripiprazole), which despite containing common toxicophore(s), display markedly different safety profiles.

Antidepressant therapy with nefazodone has been associated with idiosyncratic hepatic ADRs including necrosis and failure, often resulting in liver transplantation or death; liver biopsy results have been consistent with toxic injury (García-Pando et al., 2002; Stewart, 2002; Choi, 2003; Andrade and Lucena, 2003). Circumstantial evidence that reactive intermediates may be ultimately responsible for liver injury has been

DMD # 20545

presented. In humans, the oxidative pathway of nefazodone metabolism to *para*-hydroxynefazodone (**1**), a major circulating metabolite (Mayol et al., 1994), results in a *para*-hydroxyaniline analog and well-established toxicophore, which undergoes P4503A4-mediated bioactivation to electrophilic quinonoid intermediates in human liver microsomes; the structure of these reactive metabolites was inferred through the characterization of the corresponding glutathione (GSH) conjugates (Figure 1) (Kalgutkar et al., 2005b). Additionally, reactive iminium ion intermediates arising from α -carbon oxidation (adjacent to the piperazine ring nitrogen) in nefazodone and its downstream metabolites also have been characterized in rat liver microsomes as the corresponding cyano conjugates (Figure 1) (Argoti et al. 2005).

The lack of reports on nefazodone-like hepatotoxicity with the atypical antipsychotic aripiprazole is intriguing. Since its introduction in 2003, aripiprazole has enjoyed great commercial success in the treatment of schizophrenia with 2006 revenues exceeding one billion US dollars. Like nefazodone, P4503A4-mediated aromatic hydroxylation on the arylpiperazine motif in aripiprazole results in the formation of the *para*-hydroxyaripiprazole metabolite (aripiprazole metabolism data submitted by the manufacturer of the drug to the FDA, for a review, see: Caccia, 2007), which is capable of undergoing bioactivation to the corresponding quinone-imine/quinone intermediates (Figure 2, pathway A). In addition, the piperazine ring in aripiprazole can succumb to α -carbon oxidation resulting in the formation of reactive iminium ion intermediates (Figure 2, pathway B). Furthermore, unlike nefazodone, aripiprazole contains an acetanilide motif, capable of undergoing a bioactivation sequence involving *ortho*- or *para*-aromatic hydroxylation followed by oxidation to the quinone-imine intermediate (Figure 2,

DMD # 20545

pathway C) in a manner similar to that observed with acetaminophen (Hinson, 1983). Finally, dehydroaripiprazole (Figure 2, pathway D), the active metabolite of aripiprazole (Molden et al., 2006), is a α,β -unsaturated carbonyl compound and can potentially react directly with GSH (Figure 2, pathway E) or undergo oxidation on the double bond forming an electrophilic epoxide that can react with GSH (Figure 2, pathway F). Pathway F depicted in figure 2 is known to occur on the quinolinone ring in the inotropic agent toborinone (see Figure 2) (Kitani et al., 1997).

Since detailed information on the overall biotransformation pathways of aripiprazole in humans including the potential for bioactivation is currently unavailable in the primary literature, we decided to characterize the *in vitro* metabolic/bioactivation pathways of aripiprazole in human liver microsomes. Nefazodone was included as a positive control in these studies. Special emphasis was placed on the characterization of reactive iminium species of nefazodone in human liver microsomes, since previous information on this bioactivation pathway was limited to the rat (Argoti et al., 2005). Studies comparing the inhibition (reversible and time-dependent) of P450 enzymes involved in aripiprazole and nefazodone metabolism were also undertaken, since time-dependent, irreversible inactivation can also be caused by covalent modification of P450 enzyme(s) that catalyze bioactivation.

Materials and Methods

Chemicals. All chemicals and solvents were purchased from the Aldrich Chemical Co. (Milwaukee, WI). Nefazodone hydrochloride, NADPH, GSH and potassium cyanide were purchased from Sigma-Aldrich (St. Louis, MO). Aripiprazole and dehydroaripiprazole were synthesized at Pfizer Global Research and Development.

DMD # 20545

Pooled human liver microsomes and recombinant human P4503A4 and P4502D6 isozymes, coexpressed with NADPH-P450 oxidoreductase in baculovirus-insect cells, were purchased from BD Gentest (Woburn, MA).

Metabolism Studies. Stock solutions of nefazodone, aripiprazole and dehydroaripiprazole were prepared in methanol or DMSO:acetonitrile (25:75, %v/v), respectively. The final concentration of organic solvent in the incubation media was 0.2% (v/v). Incubations were carried out at 37 °C for 60 min in a shaking water bath. The incubation volume was 1 ml and consisted of the following: 0.1 M potassium phosphate buffer (pH 7.4) containing MgCl₂ (10 mM), human liver microsomes (P450 concentration = 0.5 μM) or recombinant enzymes (25 pmols of P4503A4 or P4502D6), NADPH (1.2 mM), substrate (20 μM for metabolite identification and 100 μM for reactive metabolite trapping), and GSH (5 mM) or potassium cyanide (5 mM). Incubations that lacked either NADPH or trapping agents served as negative controls, and reactions were terminated by the addition of ice-cold acetonitrile (1 ml). The solutions were centrifuged (3,000 x g, 15 min) and the supernatants were dried under a steady nitrogen stream. The residue was reconstituted with mobile phase and analyzed for metabolite formation by liquid chromatography tandem mass spectrometry (LC-MS/MS).

Metabolite Identification Using Triple Quadrupole Linear Ion Trap LC-MS/MS.

A bioanalytical methodology similar to the one described by Zheng et al. (2007) was used for characterization of metabolites including GSH and/or cyano conjugates. The LC system consisted of Shimadzu LC20AD pumps, DGU20A5 degasser and VP Option box (Columbia, MD), an HTC PAL autosampler (Leap Technologies, Cary, NC), and a Phenomenex Synergi POLAR-RP HPLC column (4.6 × 150 mm, 4 μm (Phenomenex,

DMD # 20545

Torrance, CA). LC mobile phase A was 10 mM ammonium formate: IPA: formic acid in water (98.9:1.0:0.1, % v/v), and mobile phase B was formic acid in acetonitrile (0.1%). The flow rate was 0.7 ml/min. The LC gradient started at 5% B for 5 min, ramped linearly to 50% B over 30 min, increased to 90% B over 5 min, and then returned to the initial condition over 1.0 min. Post-column flow was split such that mobile phase was introduced into the mass spectrometer via an electrospray interface at a rate of 175 μ l/min. The remaining flow was diverted to the PDA detector to provide simultaneous UV detection ($\lambda = 254$ nm) and total ion chromatogram. The LC system was interfaced to an API 4000 Q-trap mass spectrometer (Sciex, Toronto, Canada) equipped with the Turboionspray source. Metabolites including GSH and cyano conjugates were initially characterized in the full scan mode (from m/z 100 to 850) by comparing $t = 0$ samples to $t = 60$ min samples (with or without cofactor or trapping agent), and structural information was generated from the collision-induced dissociation (CID) spectra of the corresponding protonated molecular ions. To improve sensitivity, metabolites, GSH and cyano adducts were also characterized using the multiple reaction monitoring-enhanced product ion (MRM-EPI) mode following preset MRM transitions derived from the CID information. In the case of GSH and cyano adducts these MRM transitions corresponded to the loss of the pyroglutamic acid moiety (129 Da) and cyanide (27 Da), respectively, from the molecular weight (MH^+) of the conjugate(s). In the MRM analysis, the source temperature was set at 350 $^{\circ}$ C, and the ionspray voltage was set to 5.0 kV. Nitrogen was used as the nebulizer and auxiliary gas. The dwell times for MRM analysis (up to 12 transitions) were 150 ms, and the interscan pause time for all MRM analysis was 5 ms. The same declustering potential (30 V), collision energy (50 eV), and a collision energy

DMD # 20545

spread (± 15 eV) were applied for all potential GSH and cyano adducts in the MRM-EPI mode.

P450 Inhibition Studies in Human Liver Microsomes. For non-preincubation (time-independent) inhibition of P4503A4 activity, a pooled human liver microsomal preparation (0.01 mg/ml) was incubated with midazolam (3 μ M) and test compound (nefazodone or aripiprazole) at concentrations ranging from 0.5 to 50 μ M at 37 $^{\circ}$ C for 20 min in the presence of NADPH (1.3 mM). For preincubation-dependent (time-dependent) P4503A4 inhibition, microsomes (0.01 mg/mL), NADPH (1.3 mM) and test compound (nefazodone or aripiprazole) at concentrations ranging from 0.5 to 50 μ M were incubated for 30 min at 37 $^{\circ}$ C, after which further incubation with midazolam (3 μ M) and a second aliquot of NADPH (1.3 mM) was carried out for an additional 20 min. In separate studies, reversible and time-dependent inhibition of P4502D6 activity in human liver microsomes by aripiprazole (0.5-50 μ M) was also examined in an identical fashion using the selective probe P4502D6 substrate dextromethorphan (25 μ M). All inhibition studies were conducted in triplicate. Incubations were quenched by the addition of 2 volumes of acetonitrile containing levallorphan (100 ng/ml) as internal standard. Remaining P4503A4 and P4502D6 activity as measured by the formation of 1'-hydroxymidazolam and dextrophan, respectively, was determined by LC-MS/MS using previously described bioanalytical conditions (Kalgutkar et al., 2005b, Bertelsen et al., 2003). For all HPLC analysis, peak areas of the metabolite (1'-hydroxymidazolam or dextrophan) were expressed as a ratio to the internal standard (levallorphan) peak area for each concentration of the inhibitor. These peak area ratios represent the remaining midazolam-

DMD # 20545

1'-hydroxylase and dextromethorphan demethylase activity in the microsomes and were expressed as a percentage of the time-matched control samples without inhibitor.

Results

Metabolic Profile of Nefazodone and Aripiprazole in Human Liver Microsomes.

The metabolism of nefazodone has been studied extensively in vitro (Kalgutkar et al., 2005b; Peterman et al., 2005; Li et al., 2007) and in vivo (Mayol et al., 1994). In the current investigation, we re-assessed nefazodone metabolism in human liver microsomes for comparative purposes only. Figure 3 indicates the metabolic profile of nefazodone in NADPH-supplemented human liver microsomes. The molecular ions (MH^+), MS/MS fragmentation pattern and plausible structures of the various nefazodone metabolites (M1-M11) are depicted in Table 1. The formation of metabolites M1-M7 and M9 is consistent with previously published findings and requires no further discussion (Mayol et al., 1994; Kalgutkar et al., 2005b; Peterman et al., 2005; Li et al., 2007). Three new nefazodone metabolites M8, M10 and M11 were also observed in this study. The presence of fragment ions at m/z 274 and 246 in the mass spectra of dihydroxylated metabolite M8 ($MH^+ = 502$) and monohydroxylated metabolite M11 ($MH^+ = 486$), respectively, suggested that the *N*-propyl-5-ethyl-2,4-dihydro-4-(2-phenoxyethyl)-triazolone substituent was unmodified. In contrast, the fragment ions at m/z 274 and 246 in the dihydroxylated metabolite M10 shifted by 16 Da to m/z 290 and 262, respectively, suggesting that one site of hydroxylation was on the *N*-propyl-5-ethyl-2,4-dihydro-4-(2-phenoxyethyl)-triazolone motif. In M8, the fragment ion at m/z 241 (see Table 1) indicated that both hydroxylations had occurred on the 3-chlorophenylpiperazine ring.

DMD # 20545

The fragment ion at m/z 223 (loss of 18 mass units from m/z 241) suggests that one site of hydroxylation is the phenyl ring and the other site is on the piperazine ring. Likewise, with M10 and M11, the 18 Da shift in the fragment ion at m/z 225 to m/z 207 was also consistent with piperazine ring oxidation. Treatment of the incubation mixture with the reducing agent $TiCl_3$ led to the disappearance of the peaks suggesting that they were N-oxides. Finally, the assigned regiochemistry for hydroxylations on the phenyl ring in M8 and the ethyl group in M10 is based on the information available from previously characterized nefazodone metabolites (Peterman et al., 2005).

Figure 4 shows chromatograms of the MS total ion current and UV absorption ($\lambda = 254$ nm) for extracts from NADPH-supplemented human liver microsomal incubations with aripiprazole (20 μ M). The CID spectrum of aripiprazole ($MH^+ = 448$) is revealed in Figure 5. The molecular ions (MH^+), MS/MS fragmentation pattern and plausible structures of the various aripiprazole metabolites (M12-M19) are depicted in Table 2. The molecular weights of M14 and M12 correspond to that of the 2,3-dichlorophenylpiperazine and the *para*-hydroxy-2,3-dichlorophenylpiperazine metabolites, which have been characterized previously (Caccia et al., 2007). The molecular weight of M13 was consistent with a dihydroxylated aripiprazole metabolite. The fragment ions at m/z 301 and 259 in the CID spectrum of M13 were derived from addition of 16 Da to the fragment ions at m/z 285 and m/z 243 in the CID spectrum of aripiprazole. This observation suggested the 2,3-dichlorophenylpiperazine and the dihydroquinolinone ring systems as the sites of hydroxylation. The molecular weight and CID spectrum of metabolite M15 reflected O-dealkylation of the ether linkage in aripiprazole. The molecular weights of metabolites M16 and M17 were consistent with

DMD # 20545

aripiprazole mono-hydroxylation. Fragment ions at m/z 301 and m/z 259 in the CID spectrum of M16 were consistent with monohydroxylation on the 2,3-dichlorophenylpiperazine ring system in the parent compound. In contrast, the observation that the fragment ion at m/z 285 was retained in the CID spectrum of M17 indicated monohydroxylation on the dihydroquinolinone core. The molecular weight and CID spectrum of M19 was consistent with that previously reported for dehydroaripiprazole (Molden et al., 2006). Finally, metabolite M18 was derived from the monohydroxylation of dehydroaripiprazole M19 and CID data suggested the site of monohydroxylation to be on the dehydroquinolinone motif.

Reactive Metabolite Formation: Nefazodone. *Glutathione Conjugates.* LC-MS/MS analysis of NADPH-supplemented human liver microsomal incubations containing nefazodone and GSH led to the detection of two conjugates GS1 and GS2 with molecular ions (MH^+) at 807 (retention time (R_t) = 25.89 min) and 791 (R_t = 28.66 min), respectively (Figure 6, panel A). These conjugates were not observed when NADPH and/or GSH were omitted from the incubation mixture. The molecular weights of GS1 and GS2 were consistent with the addition of one molecule of GSH to dihydroxylated and monohydroxylated nefazodone metabolites, respectively. The CID spectrum of GS1 (Figure 6, panel B) displayed diagnostic fragment ions at m/z 678, 534 and 290. The fragment ion at m/z 678 corresponded with the loss of the pyroglutamate moiety, which represents a characteristic fragment ion derived from GSH conjugates (Baillie and Davis, 1993). Likewise, the fragment ion at m/z 534 was assigned as cleavage of the cysteinyl thioether moiety with the retention of sulfur on the drug molecule. Finally, the presence of the fragment ion at m/z 290 (addition of 16 Da to the fragment ion at m/z 274 present

DMD # 20545

in parent nefazodone) indicated monohydroxylation on the *N*-propyl-5-ethyl-2,4-dihydro-4-(2-phenoxyethyl)-triazolone substituent in nefazodone. This observation also suggests that the second hydroxylation site is on the 3-chlorophenylpiperazine ring. Based on this information, the proposed structure for GS1 that fits the CID data is shown in Figure 6, panel B. The regiochemical assignments for the aromatic and aliphatic hydroxylations in GS1 are based on the previously characterized dihydroxylated metabolite of nefazodone in human liver microsomes (Peterman et al., 2005; Li et al., 2007). Finally, the CID spectrum of GS2, which displayed fragment ions at m/z 662, 518, 274 and 140, was identical to the CID spectrum of the GSH conjugate of *para*-hydroxynefazodone (structure **1** in Figure 1) (Kalgutkar et al., 2005b). As shown in Figure 1, GS2 is formed via addition of GSH to the reactive quinone-imine metabolite of *para*-hydroxynefazodone.

Cyanide Conjugates. Incubations of nefazodone in NADPH-supplemented human liver microsomes in the presence of potassium cyanide led to the detection of several cyano conjugates CN1-CN6, which were not observed when NADPH and/or cyanide were omitted from the incubation mixture (Figure 7). These conjugates were also observed in nefazodone incubations with NADPH-supplemented recombinant P4503A4 (data not shown). The molecular ions (MH^+), MS/MS fragmentation pattern and plausible structures of CN1–CN6 are depicted in Table 3 (a characteristic neutral loss of HCN (27 Da) was observed under the CID conditions for all conjugates). In all cases, MS/MS data was consistent with the addition of cyanide ion across the piperazine ring system.

DMD # 20545

For cyanide conjugates CN1, CN2 and CN3 derived from the N-dearylated metabolites of nefazodone, MS/MS data indicated the addition of cyanide (27 Da) and an additional 14 mass units to the piperazine ring. The 14 mass units appear to be consistent with an additional enzymatic step involving oxidation of the piperazine ring to the corresponding lactam metabolite. An identical finding was also reported by Argoti et al. (2005) in their characterization of the cyanide adducts of N-dearylated nefazodone metabolites in rat liver microsomes. Thus the molecular weight of CN2 ($MH^+ = 399$, $m/z = 274$, 246) was consistent with the addition of one molecule of cyanide to the N-dearylated nefazodone M3 (see Table 1) plus the 14 Da mass addition to the piperazine ring. The MH^+ at 415 for CN1 suggested the addition of 16 Da to the molecular mass of CN2. Comparison of the mass spectrum of CN1 with that of CN2 revealed a shift in the fragment ion at m/z 274 (phenoxyethyl-5-ethyltriazolone-ethyl moiety) for CN2 to m/z 290 in CN1, indicating monooxygenation of the 5-ethyltriazolone moiety. Based on the known metabolic profile of nefazodone in humans, we speculate that the site of hydroxylation in CN1 is on the secondary carbon of the ethyl group as shown in Table 3. Conjugate CN3 displayed MH^+ at 413, 14 Da higher than the MH^+ for CN2 and 2 Da lower than the MH^+ for CN1. Comparison of the mass spectrum of CN1 and CN3 revealed a 2 Da decrease in the fragment ion at m/z 290 in CN1 to m/z 288 in CN3. This finding suggests that CN3 is presumably derived from the further oxidation of the secondary alcohol functionality in CN1 resulting in the formation of the corresponding ketone.

The MH^+ at m/z 527 for CN4 was consistent with the addition of one molecule of cyanide (27 Da) to a dihydroxylated nefazodone metabolite. The fragment ions at m/z

DMD # 20545

194 and m/z 274, which correspond to the 3-chlorophenylpiperazine and the phenoxyethyl-5-ethyltriazolone-ethyl substituents in the parent compound, shifted by 16 Da, to m/z 210 and 290, respectively, suggestive of oxidation on both these regions of the nefazodone molecule. The proposed structure of CN4, which is consistent with the mass spectral data, is shown in Table 3. Indicated regiochemistry of aromatic and aliphatic hydroxylation is assumed, based on the previous structural characterization of the dihydroxynefazodone metabolite (Peterman et al., 2005; Li et al., 2007). The MH^+ at m/z 511 for CN5 and CN6 (see Table 3 for structures) was consistent with the addition of one molecule of cyanide (27 Da) to a monohydroxylated nefazodone metabolite. With CN5, the fragment ions at m/z 274 and 246, which correspond to the phenoxyethyl-5-ethyltriazolone-ethyl moiety remained intact but the fragment ion at m/z 194 shifted by 16 Da to m/z 210 consistent with oxygenation on the 3-chlorophenylpiperazine ring. In contrast, with CN6, the fragment ions at m/z 274 and 246, shifted by 16 Da, to m/z 290 and 262, respectively, which suggested monooxygenation of the 5-ethyltriazolone substituent.

Aripiprazole. GSH Conjugates. LC-MS/MS analysis of NADPH-supplemented human liver microsomal incubations containing aripiprazole and GSH led to the detection of a single conjugate GS3 ($R_t = 28.07$ min) with a molecular ion (MH^+) at 769 Da (Figure 8, panel A). The formation of GS3 was also assessed using recombinant P4503A4 and P4502D6 enzymes, which are involved in aripiprazole metabolism. GS3 was detected in aripiprazole incubations with recombinant P4503A4 (Figure 8, panel B) but not P4502D6. The molecular weight of GS3 was consistent with the addition of one molecule of GSH to a monohydroxylated aripiprazole metabolite. The CID spectrum of GS3

DMD # 20545

(Figure 8, panel C) displayed diagnostic fragment ions at m/z 640, 496, 463, 285 and 243. The fragment ion at m/z 640 and 496 were assigned to the characteristic losses of pyroglutamate and C-S bond cleavage with retention of sulfur on the aripiprazole molecule. The fragment ions at m/z 285 and 243 suggest that monohydroxylation and GSH conjugation had occurred on the dihydroquinolinone core. Two plausible structures (A and B) of GS3, which are consistent with the CID spectrum are shown in Figure 8, panel C. As depicted in figure 2, structure A is derived from the aripiprazole bioactivation pathways D and F, while structure B is derived from bioactivation pathway C.

The availability of the synthetic standard of dehydroaripiprazole (metabolite M19) allowed additional studies to be conducted, which provided further insight into the structure of GS3. As shown in Figure 9 (panel B), LC-MS/MS analysis of an incubation mixture of dehydroaripiprazole in NADPH-supplemented human liver microsomes in the presence of GSH indicated the formation of a GSH conjugate GS4. The observed molecular ion (MH^+) at 767 Da and R_t of GS4 were different from that for GS3 (Figure 9, panel A). The molecular weight of GS4 was 2 Da lower than that of GS3. The CID spectrum of GS4, which is shown in Figure 9, panel C, displayed diagnostic fragment ions at m/z 638, 494 and 285. The fragment ion at m/z 285 indicated that monohydroxylation and GSH conjugation had occurred on the dehydroquinolinone core. The fragment ions at m/z 638 and 494 were assigned to the characteristic losses of pyroglutamate and C-S bond cleavage with retention of sulfur on the aripiprazole molecule. Based on these observations, a structure for GS4, which is consistent with the mass spectrum is shown in Figure 9, panel C. Thus, GS4 is a structural analog of GS3

DMD # 20545

and the formation of these conjugates appears to be derived from hydroxylation *para* (or *ortho*) to the quinolinone nitrogen atom in aripiprazole (or dehydroaripiprazole) followed by: (a) two-electron oxidation to the electrophilic quinone-imine derivatives and (b) Michael addition of GSH to these quinone-imine intermediates. Finally, it is noteworthy to point out that while NADPH- and GSH-supplemented incubations of dehydroaripiprazole did not give rise to GS3, we did observe a metabolite M20 ($MH^+ = 480$, $R_t = 34.78$ min) derived from the dihydroxylation of dehydroaripiprazole. The CID of M20 (Figure 10, panel B) was consistent with dihydroxylation of the olefinic bond within the dehydroquinolinone moiety.

Cyanide Conjugates. Incubations of aripiprazole in NADPH-supplemented human liver microsomes in the presence of potassium cyanide did not reveal the formation of cyanide adducts.

Inhibitory Effect on P450 Activity in Human Liver Microsomes. Inhibition studies were repeated with nefazodone, since the present set of experiments utilized a much lower human liver microsomal concentration of 0.01 mg/ml to minimize non-specific binding of inhibitor to microsomes (Obach et al., 2007). Our previous studies with nefazodone were conducted with a microsomal concentration of 0.8 mg/ml (Kalgutkar et al., 2005b). Consistent with our previous results, nefazodone was a potent, concentration and time-dependent inhibitor of P450A4-mediated midazolam-1'-hydroxylase activity in human liver microsomes. The magnitude of enzyme inhibition was higher when the experiment was carried out with preincubation in the presence of NADPH. The IC_{50} value for the time-independent and time-dependent inhibition of

DMD # 20545

P4503A4 activity by nefazodone was 1.5 μM and 0.015 μM , respectively. Under the present assay conditions, the IC_{50} value for the time-independent and time-dependent inhibition of P4503A4 activity in human liver microsomes by aripiprazole was 16 μM and 12 μM , respectively. Since P4502D6 is also involved in the metabolism of aripiprazole, we also assessed the ability of aripiprazole to inhibit P450 2D6-mediated dextromethorphan-*O*-demethylase activity in human liver microsomes. The IC_{50} value for the time-independent and time-dependent inhibition of P4502D6 activity by aripiprazole was 6.4 μM and 6.7 μM , respectively.

Discussion

In vitro characterization of reactive quinonoid species derived from the bioactivation of *para*-hydroxynefazodone, a circulating metabolite of nefazodone in humans, suggests a causative role for reactive metabolites in nefazodone hepatotoxicity (Kalgutkar et al., 2005b). Our present studies on nefazodone metabolism in human liver microsomes and recombinant P4503A4 revealed additional bioactivation pathways involving α -carbon oxidation on the piperazine ring in nefazodone and several of its downstream metabolites, yielding reactive iminium ion intermediates. Argoti et al. (2005) have also reported a similar finding following nefazodone incubations with rat liver microsomes. Overall, the observations that nefazodone bioactivation by P4503A4 results in the mechanism-based inactivation of the isozyme presumably via covalent modification of an active site nucleophile(s) by reactive quinonoid and/or iminium intermediates (Kalgutkar et al., 2005b) suggests a possibility that these metabolites also can covalently modify

DMD # 20545

macromolecules other than P450, some of which, may be essential for critical pathophysiology in the liver.

Like nefazodone, P450-mediated metabolism on the 2,3-dichlorophenyl ring in aripiprazole resulted in the formation of the corresponding *para*-hydroxyaniline toxicophores as metabolites. However, the lack of formation of GSH conjugates of these metabolites suggests that they do not undergo further two-electron oxidation to electrophilic quinone-imine intermediates in an analogous manner as nefazodone. The absence of N-dearylated aripiprazole metabolites in the microsomal incubations further supports this hypothesis, since, the mechanism of N-dearylation observed with nefazodone is thought to involve hydrolytic cleavage of the reactive quinone-imine species (see Figure 1). Furthermore, unlike the case with nefazodone, we did not detect cyanide conjugates of aripiprazole and its downstream metabolites, which would be consistent with α -carbon oxidation on the piperazine ring to yield reactive iminium ions. Overall, the biochemical basis for the marked differences in the bioactivation profile involving the 3-chlorophenyl- and the 2,3-dichlorophenyl-piperazine ring systems in nefazodone and aripiprazole, respectively, remains unclear at the present time. Whether the presence of the extra chlorine atom in aripiprazole alters the electronic environment (reduces the propensity towards two-electron oxidation) of the hydroxyaniline metabolite(s) needs to be tested, experimentally. Towards achieving this goal, we have undertaken the synthesis of a nefazodone analog, which contains the additional chlorine atom on the C-2 position, in order to evaluate the propensity of this analog to form quinone-imine and/or iminium ion intermediates.

DMD # 20545

While the 2,3-dichlorophenylpiperazine ring, appeared to be latent towards bioactivation, a GSH conjugate (GS3) derived from bioactivation of the dihydroquinolinone motif in aripiprazole was detected. The molecular weight of GS3 suggested the addition of GSH to a monohydroxylated aripiprazole metabolite and the CID data indicated that this modification had occurred on the dihydroquinolinone nucleus. The formation of GS3 can arise via the two pathways C and D/F as depicted in Figure 2. The bioactivation pathway C can arise via hydroxylation *para* (or *ortho*) to the quinolinone nitrogen atom followed by: (a) two-electron oxidation to the electrophilic quinone-imine and (b) Michael addition of GSH to the quinone-imine intermediate. The bioactivation pathway D/F is analogous to the one reported for the dihydroquinolinone-containing inotropic agent toborinone (Kitani et al., 1997) and involves olefin epoxidation of the initially formed dehydroaripiprazole metabolite. Epoxide ring opening by GSH then affords GS3. The finding that NADPH- and GSH-supplemented human liver microsomal incubations of synthetic dehydroaripiprazole metabolite did not yield GS3 suggested that aripiprazole dehydrogenation is not a prerequisite for the formation of GS3 and argues against the pathways D/F. Instead, the formation of a new GSH conjugate GS4 with molecular weight 2 Da lower than that of GS3 suggests that both aripiprazole and dehydroaripiperazole succumb to an identical bioactivation pathway. Consequently on the basis of these findings, we speculate that the formation of GS3 from aripiprazole and GS4 from dehydroaripiprazole arises via the bioactivation pathway shown in Figure 2, pathway C. Within this context, it is interesting that P450-mediated oxidation of dehydroaripiprazole in human liver microsomes did result in the formation of a dihydroxylated metabolite M20 with mass spectral properties indicative of olefin di-

DMD # 20545

hydroxylation. If so, this finding is consistent with olefin epoxidation in dehydroaripiprazole followed by hydrolysis to yield the diol M20. As to why, the epoxide was not trapped by GSH remains unclear at the present time. Overall, these results constitute the first report on the P450-catalyzed bioactivation of aripiprazole. Besides literature reports on the involvement of P4503A4 in the metabolism of aripiprazole in humans, our studies also demonstrated a key role for the enzyme in the bioactivation of this drug. While both P4503A4 and P4502D6 are thought to be involved in aripiprazole metabolism (Caccia et al., 2007), we did not observe the formation of GS3 in aripiprazole incubations recombinant P4502D6. A plausible explanation for this finding may be that only P4503A4 is capable of catalyzing of aripiprazole bioactivation involving aromatic hydroxylation on the quinolinone moiety.

Given that a bioactivation pathway was detected with aripiprazole (albeit different from the one in nefazodone), we decided to compare the time-dependent P450 inhibitory potencies of nefazodone and aripiprazole. Consistent with our previous findings, the potency of P4503A4 inhibition by nefazodone significantly increased with time (~ 1000-fold increase based on the IC_{50} values of 15 μ M and 0.015 μ M for time-independent and time-dependent inhibition). The potent, time- and concentration-dependent inactivation of P4503A4 activity by nefazodone is consistent with the numerous examples of pharmacokinetic interactions of nefazodone with P4503A4 substrates and with the non-stationary pharmacokinetics of this drug due to auto-inactivation of its elimination mechanism (Greene and Barbhuiya, 1997). In contrast, aripiprazole did not display the marked time-dependent differences in P4503A4 and P4502D6 inhibitory potencies. The finding that aripiprazole is not a P4503A4 inactivator despite undergoing bioactivation

DMD # 20545

suggests that the reactive metabolite escapes the P4503A4 active site prior to the inactivation step. Alternately, it is likely that the area where the dihydroquinolinone ring resides in the P4503A4 active site lacks a nucleophilic amino acid residue(s). Despite some reversible inhibition of P4503A4 and P4502D6 activities observed in our studies, there are no reports on clinical drug-drug interactions between aripiprazole and P4503A4/P4502D6 substrates (aripiprazole package insert). The most likely explanation for this discrepancy is that the IC_{50} values for P450 isozyme inhibition by aripiprazole are significantly greater than the free maximal plasma concentrations of 2.2-8.8 nM in humans after daily oral administration of the drug for 14 days at a dose range of 5-20 mg (Mallikaajun et al., 2004).

Our findings on the P4503A4-mediated bioactivation of nefazodone and aripiprazole in human liver microsomal incubations represent a classical assessment of bioactivation potential of xenobiotics and drugs. Often time, such a finding can be interpreted as being a harbinger of a potential toxicological response in the clinic. Clearly, the hepatotoxic ADRs associated with nefazodone supports this notion. But, this is not the case with aripiprazole since despite the bioactivation liability and the fact that both drugs are intended for chronic use, there have been no reports of idiosyncratic hepatotoxicity associated with this drug. Plausible explanations for this discrepancy may be accounted by the differences in dose levels and the pharmacokinetics of the two drugs. The absolute oral bioavailability of nefazodone (Greene and Barbhैया, 1997) and aripiprazole (aripiprazole metabolism data submitted by the manufacturer of the drug to the FDA) in humans has been estimated to be ~ 20% and 87%, respectively. The low oral bioavailability of nefazodone stems from extensive first pass metabolism mediated by

DMD # 20545

P4503A4 in the small intestine and liver. The total clearance and volume of distribution at steady state of nefazodone following intravenous administration to humans is 7.5 ml/min/kg (hepatic extraction of 40% based on a human hepatic blood flow of 21 ml/min/kg) and 0.51 l/kg, which translates into a short half-life of ~ 1 hr (Barbhaiya et al., 1996). In contrast, the terminal half-life of aripiprazole is very long averaging ~ 75 hr and is a consequence of a significantly lower total clearance (0.8 ml/min/kg, hepatic extraction of < 5%) and increased volume of distribution at steady state (5 l/kg) (aripiprazole metabolism data submitted by the manufacturer of the drug to the FDA).

Given the longer half-life of aripiprazole compared with nefazodone, the daily dose is ~ 10-30-fold lower (5-20 mg once-a-day) than the daily dose of nefazodone (200-400 mg once a day). The lower daily dose and the lesser affinity towards metabolism/bioactivation likely reduces the total body burden to reactive metabolite exposure upon aripiprazole administration as compared to that following nefazodone administration. There are several examples (clozapine vs. olanzapine and troglitazone vs. rosiglitazone/pioglitazone) of structurally analogous drugs that display differential safety profiles despite forming reactive metabolites. In all of these cases, the drug(s) that is associated with idiosyncratic ADRs are dosed at considerably greater levels. For example, clozapine is dosed at 200 mg/day compared to the 10 mg/day dose of olanzapine. Overall, the studies describe herein, provide yet another example that in vitro bioactivation of a drug (or drug candidate) cannot necessarily be assumed to be predictive of toxicity. It is important to place results from in vitro bioactivation studies within the proper context of overall factors (e.g., indication, acute versus chronic therapy, dose size

DMD # 20545

and regimen) when making a final decision on whether to proceed with the development of the drug.

References

- Andrade RJ and Lucena MI (2003) Drug-induced hepatotoxicity. *N Engl J Med* **349**:1974-1976.
- Argoti D, Liang L, Conteh A, Chen L, Berhas D, Yu C-P, Vouros P and Yang E (2005) Cyanide trapping of iminium ion reactive intermediates followed by detection and structure identification using liquid chromatography-tandem mass spectrometry (LC-MS/MS). *Chem Res Toxicol* **18**:1537-1544.
- Baillie TA and Davis MR (1993) Mass spectrometry in the analysis of glutathione conjugates. *Biol Mass Spectrom* **22**:319-325.
- Barbhaiya RH, Dandekar KA and Greene DS (1996) Pharmacokinetics, absolute bioavailability, and disposition of [¹⁴C]nefazodone in humans. *Drug Metab Dispos* **24**:91-95.
- Bertelsen KM, Venkatakrishnan K, Von Moltke LL, Obach RS and Greenblatt DJ (2003) Apparent mechanism-based inhibition of human CYP2D6 in vitro by paroxetine: comparison with fluoxetine and quinidine. *Drug Metab Dispos* **31**:289-293.
- Caccia S (2007) N-Dealkylation of arylpiperazine derivatives: Disposition and metabolism of the 1-arylpiperazines formed. *Curr Drug Metab* **8**:612-622.
- Choi S (2003) Nefazodone (serzone) withdrawn because of hepatotoxicity. *CMAJ* **169**:1187.
- Evans DC, Watt AP, Nicoll-Griffith DA and Baillie TA (2004) Drug-Protein Adducts: An Industry Perspective on Minimizing the Potential for Drug Bioactivation in Drug Discovery and Development. *Chem Res Toxicol* **17**:3-16.

DMD # 20545

García-Pando AC, García del Pozo J, Sánchez AS, Martín AV, Rueda de Castro AM and Lucena MI (2002) Hepatotoxicity associated with the new antidepressants. *J Clin Psychiatry* **63**:135-137.

Gorrod JW and Aislaitner G (1994) The metabolism of alicyclic amines to reactive iminium ion intermediates *Eur J Drug Metab Pharmacokinet* **19**:209-217.

Greene DS and Barbhuiya RH (1997) Clinical pharmacokinetics of nefazodone. *Clin Pharmacokinet* **33**:260-275.

Hinson JA (1983) Reactive metabolites of phenacetin and acetaminophen: a review. *Environ Health Perspect* **49**:71-79.

Kalgutkar AS and Soglia JR (2005) Minimising the potential for metabolic activation in drug discovery. *Exp Opin Drug Metab Toxicol* **1**:91-142.

Kalgutkar AS, Gardner I, Obach RS, Shaffer CL, Callegari E, Henne KR, Mutlib AE, Dalvie DK, Lee JS, Nakai Y, O'Donnell JP, Boer J and Harriman SP (2005a) A comprehensive listing of bioactivation pathways of organic functional groups. *Curr Drug Metab* **6**:161-225.

Kalgutkar AS, Vaz AD, Lame ME, Henne KR, Soglia J, Zhao SX, Abramov YA, Lombardo F, Collin C, Hensch ZS and Hop CE (2005b) Bioactivation of the nontricyclic antidepressant nefazodone to a reactive quinone-imine species in human liver microsomes and recombinant cytochrome P450 3A4. *Drug Metab Dispos* **33**:243-253.

Kitani M, Miyamoto G, Nagasawa M, Yamada T, Matsubara J, Uchida M and Odomi M (1997) Biotransformation of the novel inotropic agent toborinone (OPC-18790) in

DMD # 20545

rats and dogs. Evidence for the formation of novel glutathione and two cysteine conjugates. *Drug Metab Dispos* **25**:663-674.

Li AC, Shou WZ, Mai TT and Jiang XY (2007) Complete profiling and characterization of in vitro nefazodone metabolites using two different tandem mass spectrometric platforms. *Rapid Commun Mass Spectrom* **21**:4001-4008.

Mallikaarjun S, Salazar DE and Bramer SL (2004) Pharmacokinetics, tolerability, and safety of aripiprazole following multiple oral dosing in normal healthy volunteers. *J Clin Pharmacol* **44**:179-187.

Mayol RF, Cole CA, Luke GM, Colson KL and Kerns EH (1994) Characterization of the metabolites of the antidepressant drug nefazodone in human urine and plasma. *Drug Metab Dispos* **22**:304-311.

Molden E, Lunde H, Lunder N and Refsum H (2006) Pharmacokinetic variability of aripiprazole and the active metabolite dehydroaripiprazole in psychiatric patients. *Ther Drug Monit* **28**:744-749.

Nelson SD (2001) Structure toxicity relationships--how useful are they in predicting toxicities of new drugs? *Adv. Exp. Med. Biol.* **500**:33-43.

Obach RS, Walsky RL and Venkatakrisnan K (2007) Mechanism-based inactivation of human cytochrome P450 enzymes and the prediction of drug-drug interactions. *Drug Metab Dispos* **35**:246-255.

Park BK, Kitteringham NR, Maggs JL, Pirmohamed M and Williams DP (2005) The role of metabolic activation in drug-induced hepatotoxicity. *Ann Rev Pharmacol Toxicol* **45**:177-202.

DMD # 20545

Peterman SM, Duczak N Jr, Kalgutkar AS, Lame ME and Soglia JR (2005)

Application of a linear ion trap/orbitrap mass spectrometer in metabolite characterization studies: examination of the human liver microsomal metabolism of the non-tricyclic anti-depressant nefazodone using data-dependent accurate mass measurements. *J Am Soc Mass Spectrom* **17**:363-375.

Stewart DE (2002) Hepatic adverse reactions with nefazodone. *Can J Psychiatry* **47**:375-377.

Zheng J, Ma L, Xin B, Olah T, Griffith Humphreys W and Zhu M (2007) Screening and identification of GSH-trapped reactive metabolites using hybrid triple quadrupole linear ion trap mass spectrometry. *Chem Res Toxicol* **20**:757-766.

Figure Legends

FIG. 1. Characterized bioactivation pathways for the antidepressant nefazodone. The α -carbon oxidation adjacent to the piperazine nitrogen resulting in a reactive iminium ion intermediate has been observed with nefazodone and several of its downstream metabolites in rat liver microsomes (Argoti et al., 2005). Regiochemistry of cyanide addition to the iminium intermediate is presently unknown. For the purposes of illustration, we have shown the iminium formation sequence as it occurs with the parent compound.

FIG. 2. Postulated bioactivation sequences for the antipsychotic agent aripiprazole.

FIG. 3. LC-MS/MS analysis of an incubation mixture containing nefazodone (20 μ M) and NADPH-supplemented human liver microsomes.

FIG. 4. Total ion chromatogram (Panel A) and UV spectrum ($\lambda = 254$ nm) (Panel B) of an incubation mixture containing aripiprazole (10 μ M) and NADPH-supplemented human liver microsomes.

FIG. 5. CID spectrum of aripiprazole.

FIG. 6. Extracted ion chromatogram (panel A) of an incubation mixture containing nefazodone (100 μ M) and NADPH-supplemented human liver microsomes in the

DMD # 20545

presence of GSH (5 mM). Panel B indicates the CID spectrum of the MH^+ ion (m/z 807) of GS1 ($R_t = 25.89$ min). The origins of the characteristic ions are as indicated. GS2 is the previously reported GSH conjugate derived from the addition of GSH to the electrophilic quinone-imine metabolite of **1** (Kalgutkar et al., 2005b).

FIG. 7. Extracted ion chromatogram of an incubation mixture containing nefazodone (100 μ M) and NADPH-supplemented human liver microsomes in the presence of potassium cyanide (5 mM).

FIG. 8. Extracted ion chromatogram of an incubation mixture containing aripiprazole (100 μ M) and NADPH-supplemented human liver microsomes (panel A) or recombinant P4503A4 (panel B) in the presence of GSH (5 mM). Panel C indicates the CID spectrum of the MH^+ ion (m/z 769) of GS3 ($R_t = 28.07$ min). The origins of the characteristic ions are as indicated. The structure depicted represents one possible regioisomer and is for illustrative purposes only.

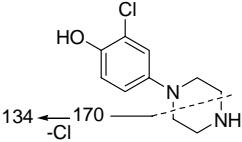
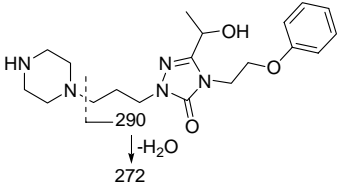
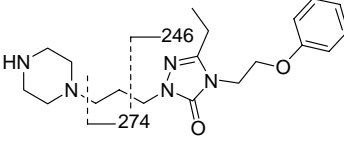
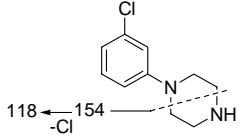
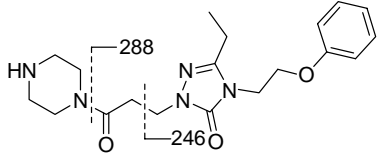
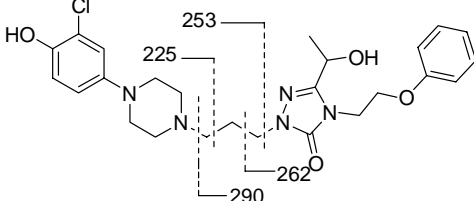
FIG. 9. Extracted ion chromatogram of an incubation mixture containing synthetic dehydroaripiprazole (100 μ M) and NADPH-supplemented human liver microsomes (panel B) in the presence of GSH (5 mM). Panel A indicates the ion chromatogram for GS3 formed in NADPH- and GSH-supplemented aripiprazole incubations. Panel C indicates the CID spectrum of the MH^+ ion (m/z 767) of GS4 ($R_t = 35.06$ min). The origins of the characteristic ions are as indicated. The structure depicted represents one possible regioisomer and is for illustrative purposes only.

DMD # 20545

FIG. 10. Extracted ion chromatogram (Panel A) of the dihydroxylated metabolite M20 formed in synthetic dehydroaripiprazole incubations in NADPH- and GSH-supplemented human liver microsomes Panel B indicates the CID spectrum of the MH^+ ion (m/z 480) of M20 ($R_t = 34.78$ min). The origins of the characteristic ions are as indicated.

TABLE 1

Molecular ions (MH⁺) and MS² fragmentation pathways of nefazodone metabolites in NADPH-supplemented human liver microsomes

Metabolite	Proposed Structure	MH ⁺ (m/z)	MS ²
M1		213	170 (100%), 134
M2		376	290 (100%), 272
M3		360	274 (100%), 246
M4		197	154 (100%), 118
M5		374	288 (100%), 246, 168, 140
M6		502	290 (100%), 262, 253, 225

DMD # 20545

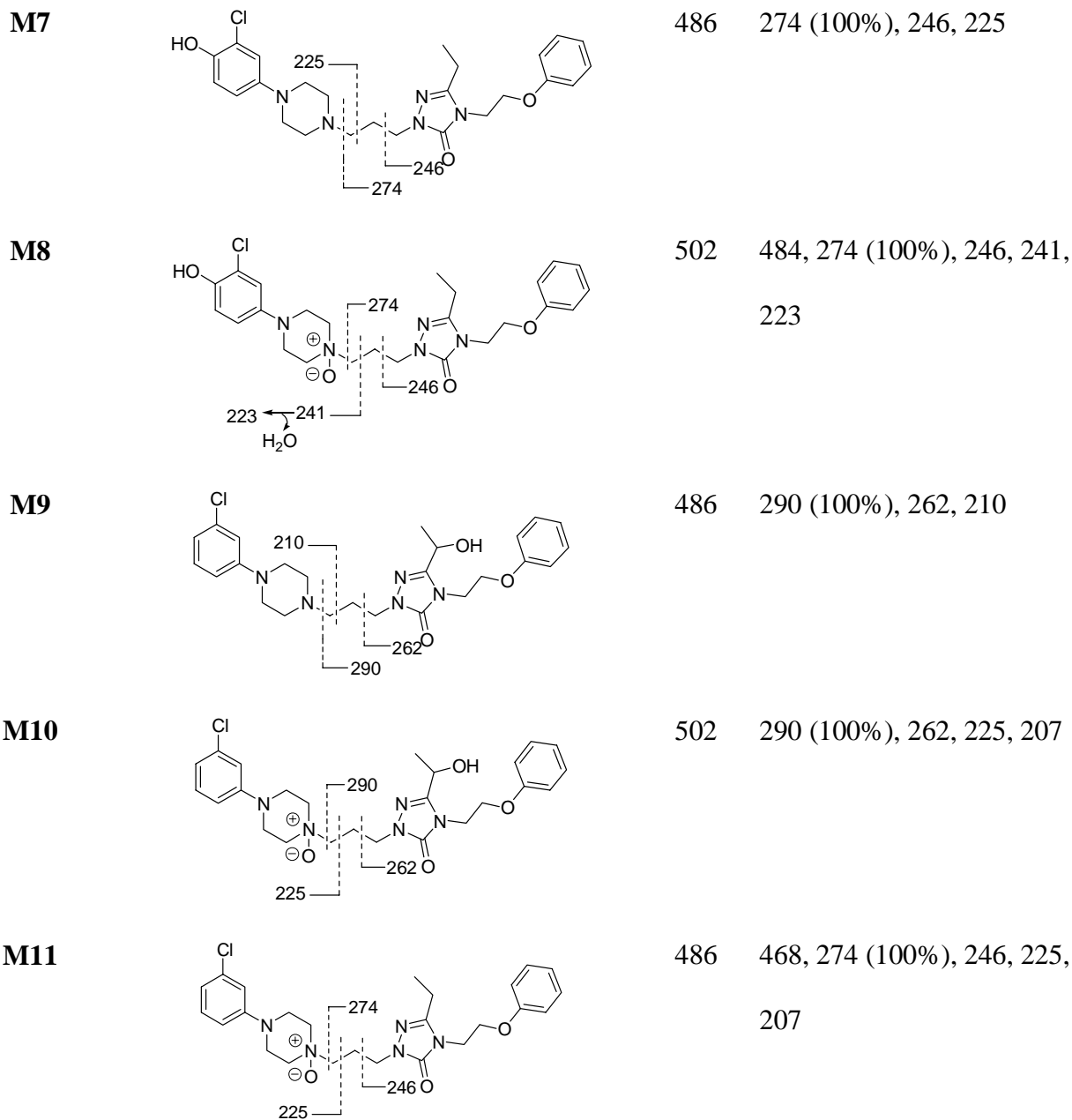
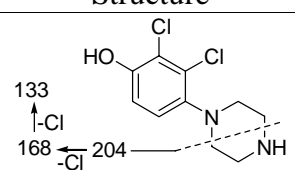
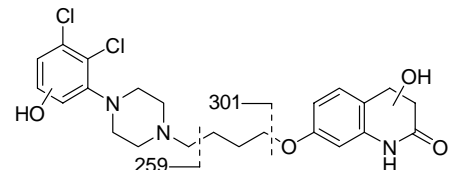
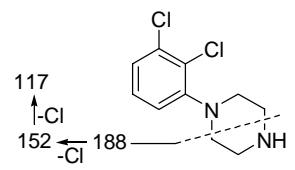
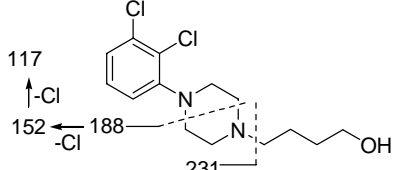
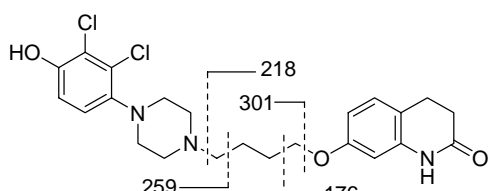
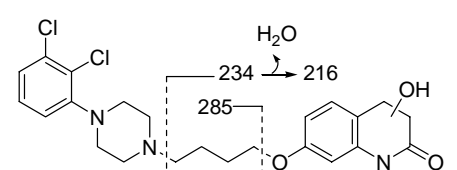


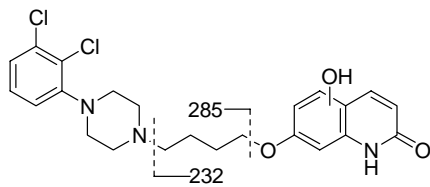
TABLE 2

*Molecular ions (MH⁺) and MS² fragmentation pathways of aripiprazole metabolites in
 NADPH-supplemented human liver microsomes*

Metabolite	Proposed Structure	MH ⁺ (m/z)	MS ²
M12		247	204, 168 (100%), 133
M13		480	462, 301 (100%), 259
M14		231	188 (100%), 152, 117
M15		303	231 (100%), 188, 152, 117
M16		464	301 (100%), 259, 218, 176
M17		464	285 (100%), 234, 216

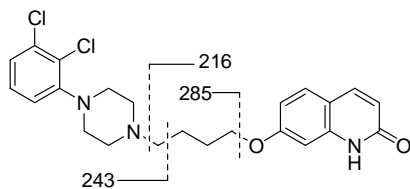
DMD # 20545

M18



462 285 (100%), 232

M19



446 285 (100%), 243, 216

TABLE 3

Molecular ions (MH⁺) and MS² fragmentation pathways of cyano adducts CN1-CN6 of nefazodone in NADPH-supplemented human liver microsomes

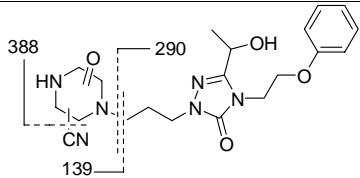
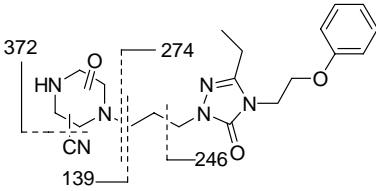
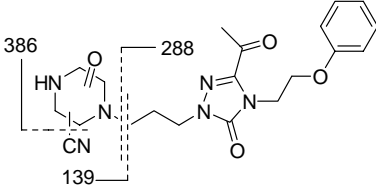
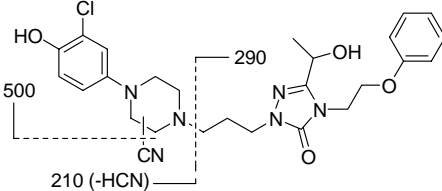
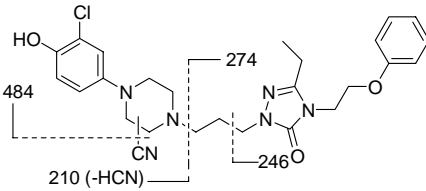
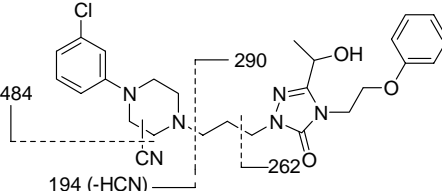
Cyano Conjugate	Proposed Structure	MH ⁺ (m/z)	MS ²
CN1		415	388, 290, 139 (100%)
CN2		399	372, 274, 246, 139 (100%)
CN3		413	386, 288, 139 (100%)
CN4		527	500 (100%), 290, 210
CN5		511	484 (100%), 274, 246, 210
CN6		511	484 (100%), 290, 262, 194

Figure 1

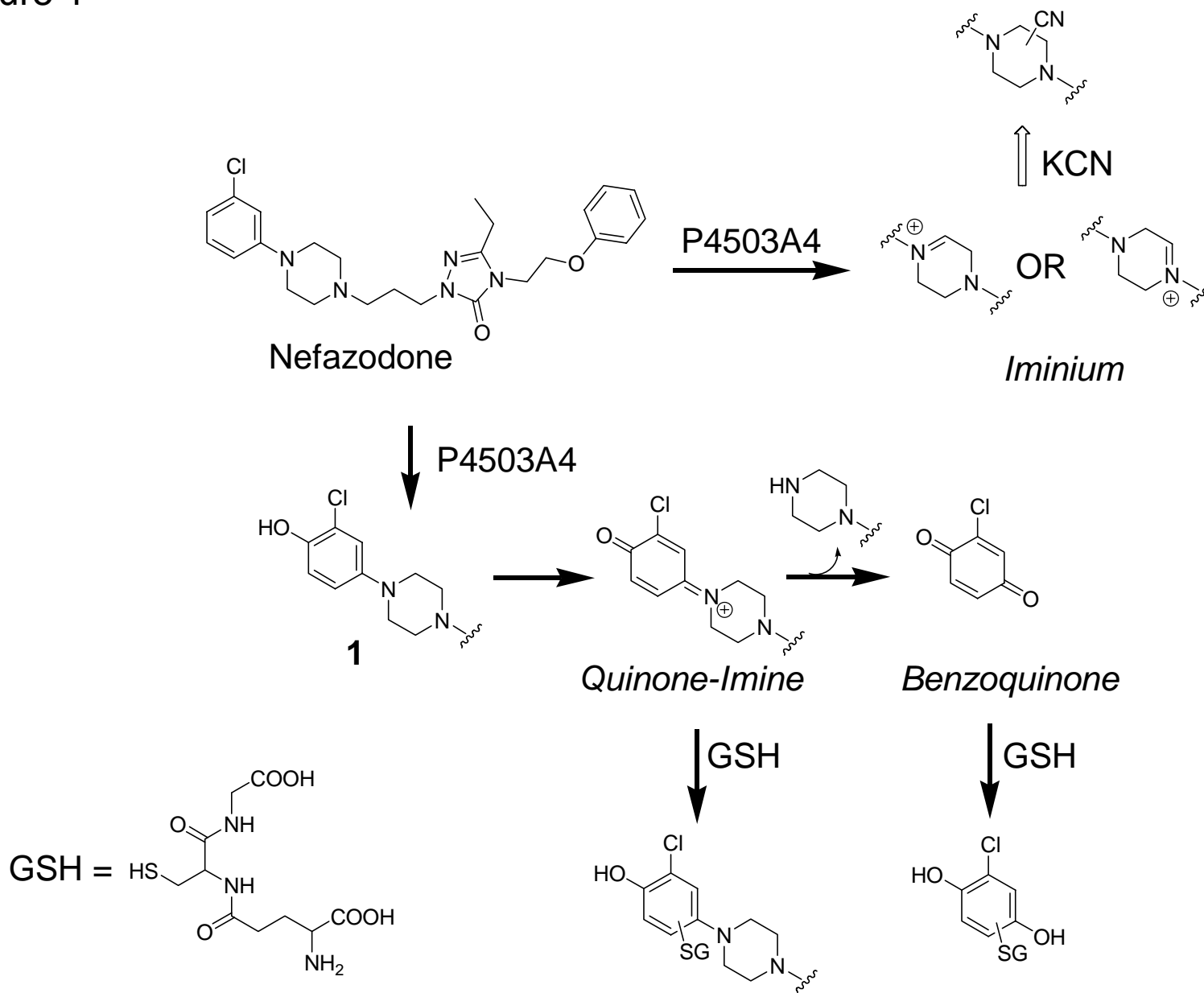


Figure 2

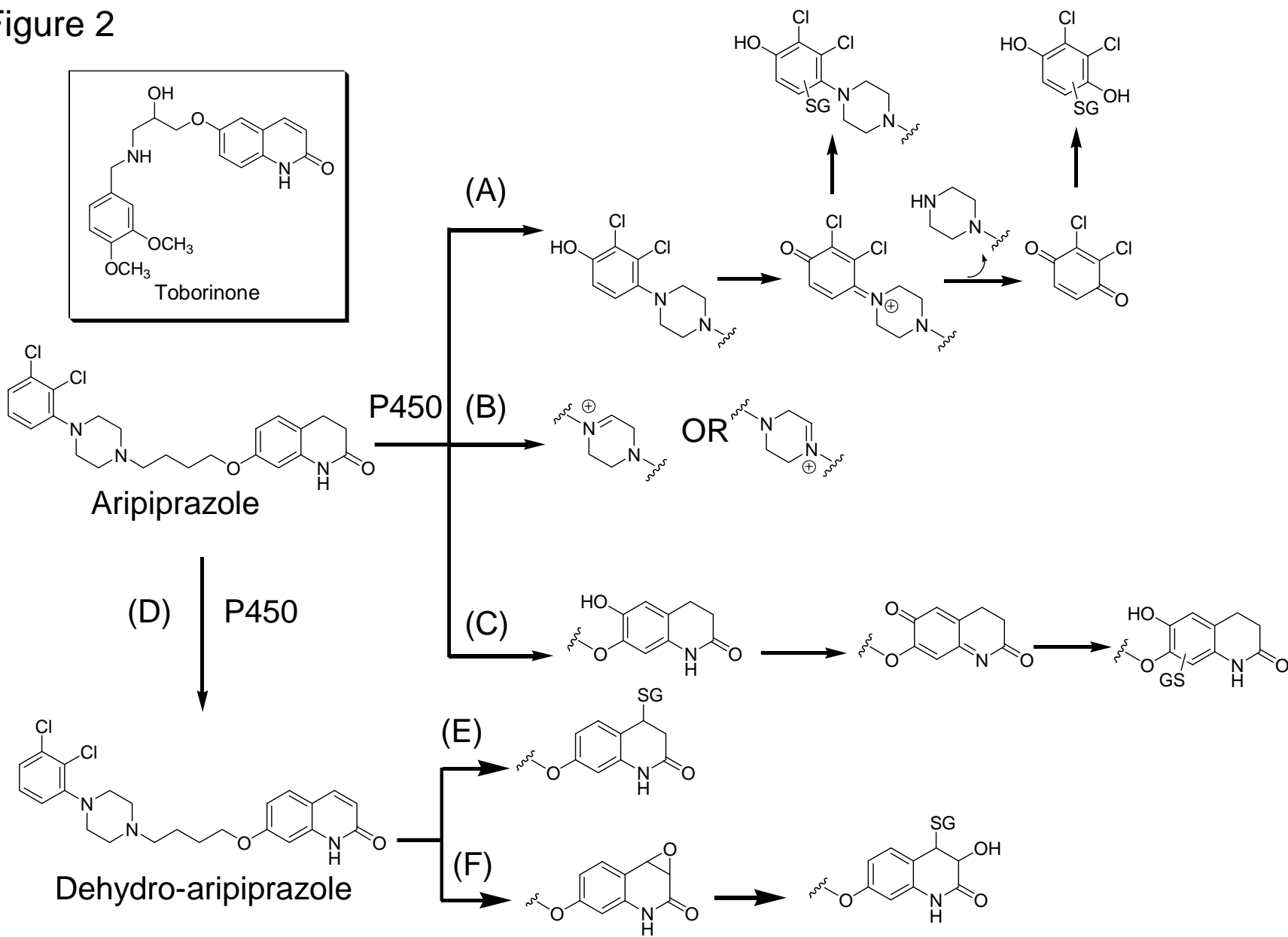


Figure 3

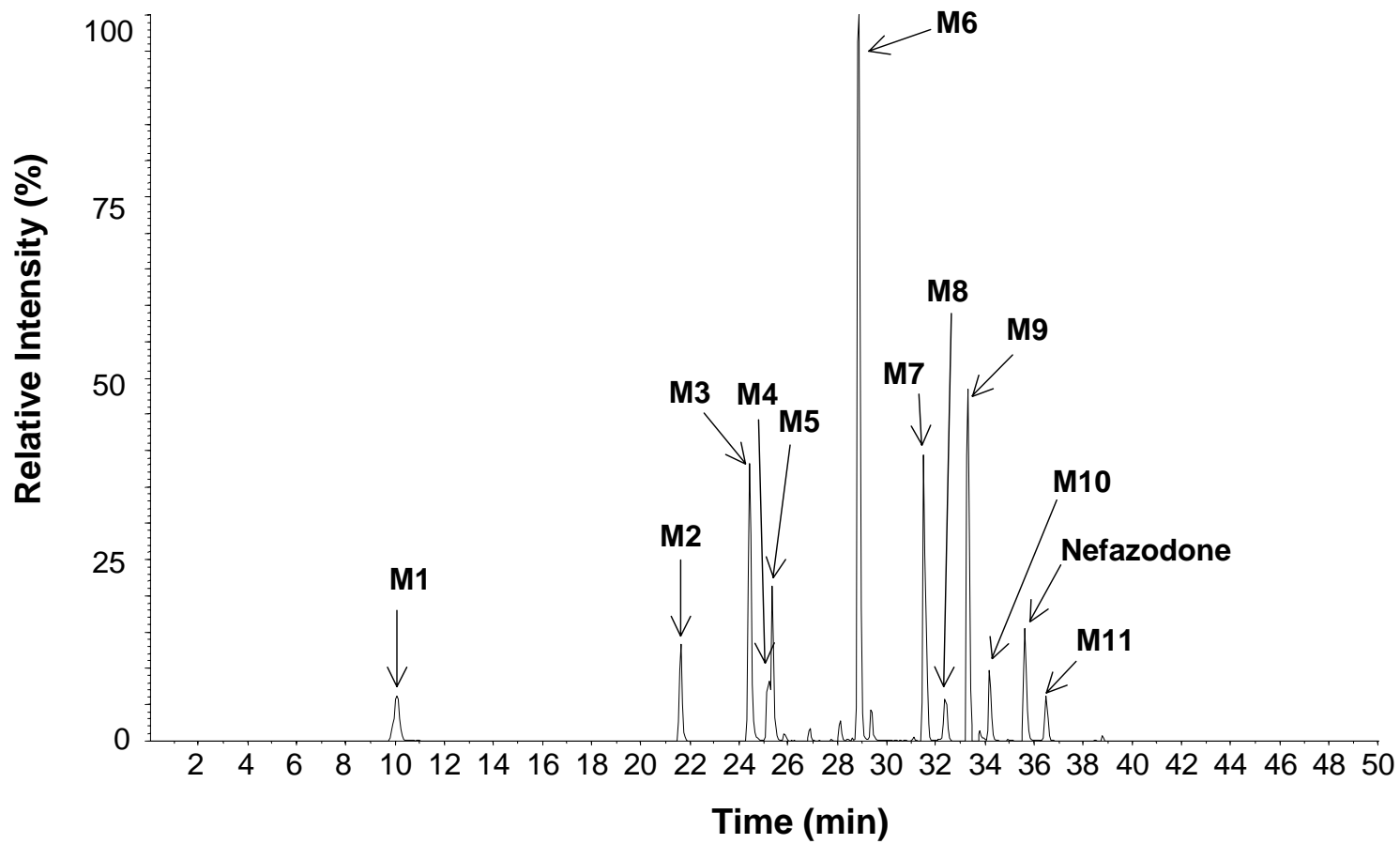


Figure 4

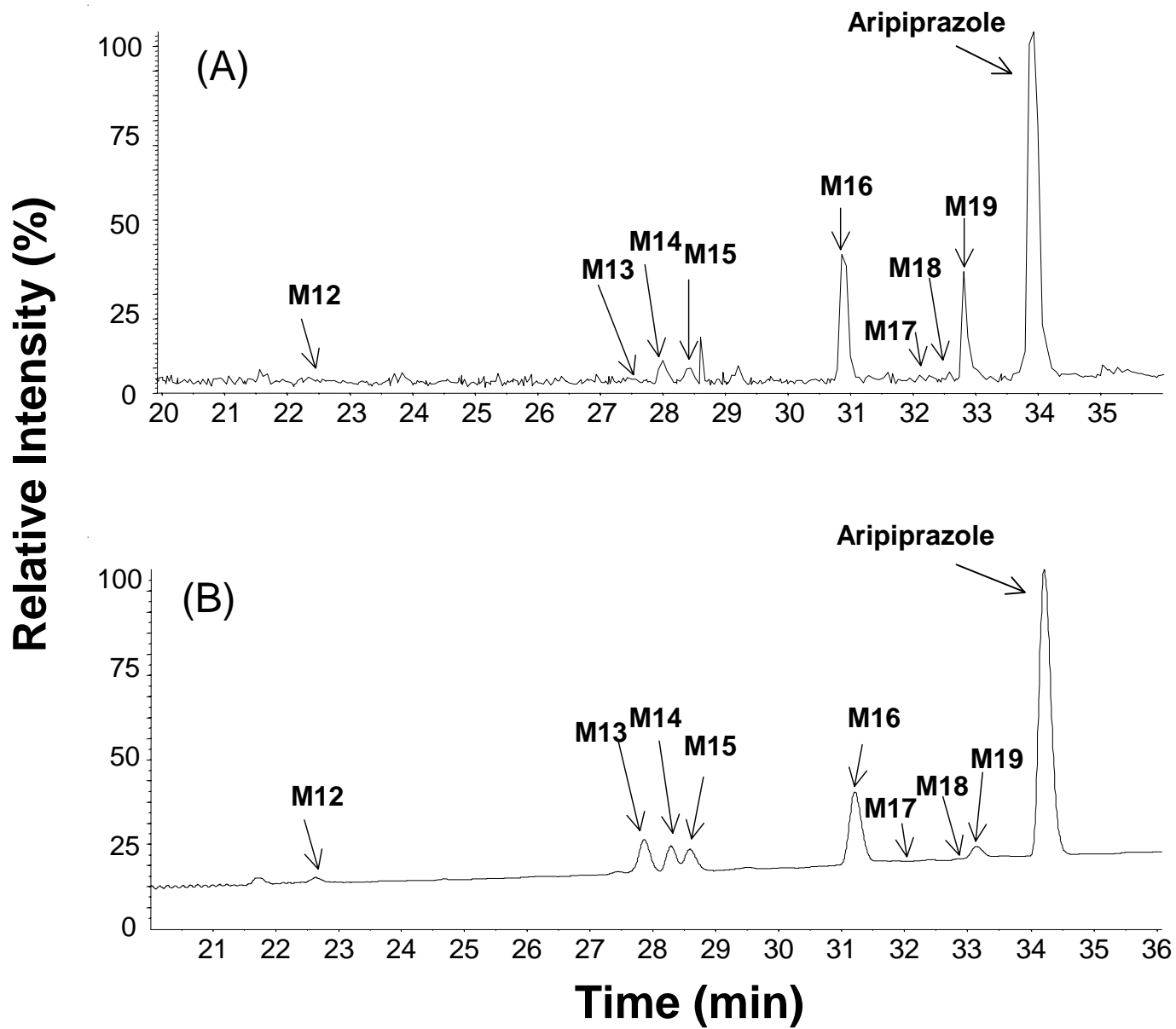


Figure 5

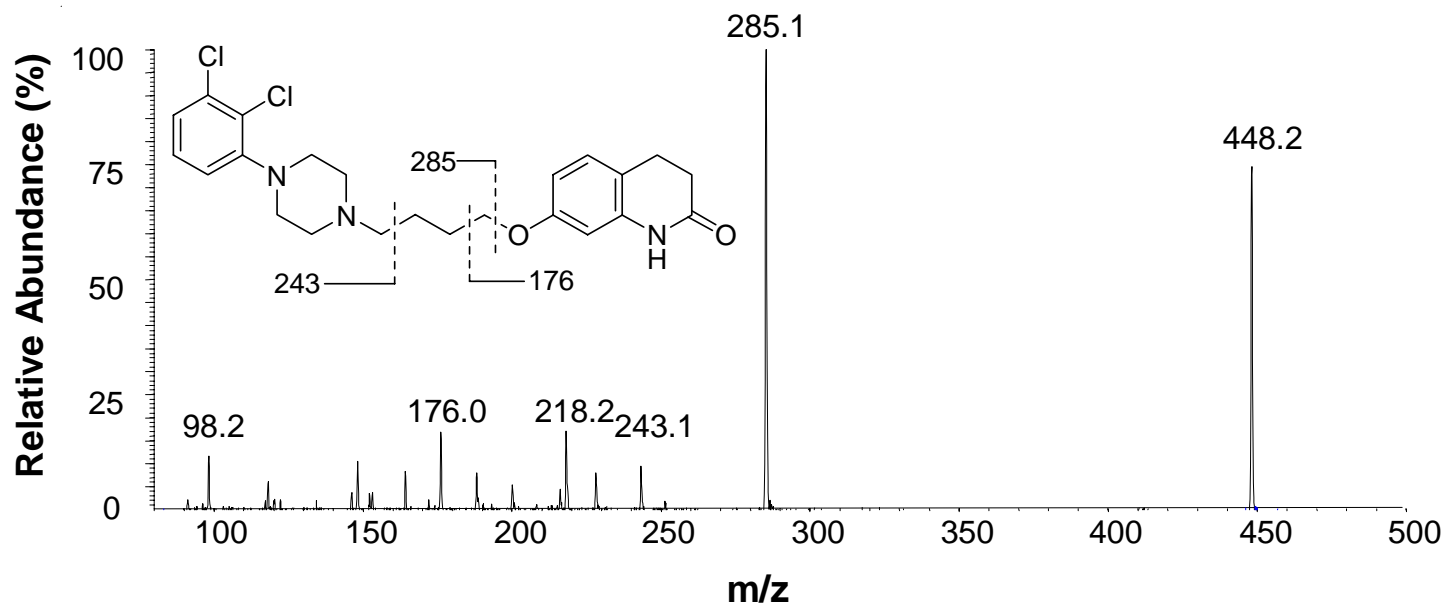


Figure 6

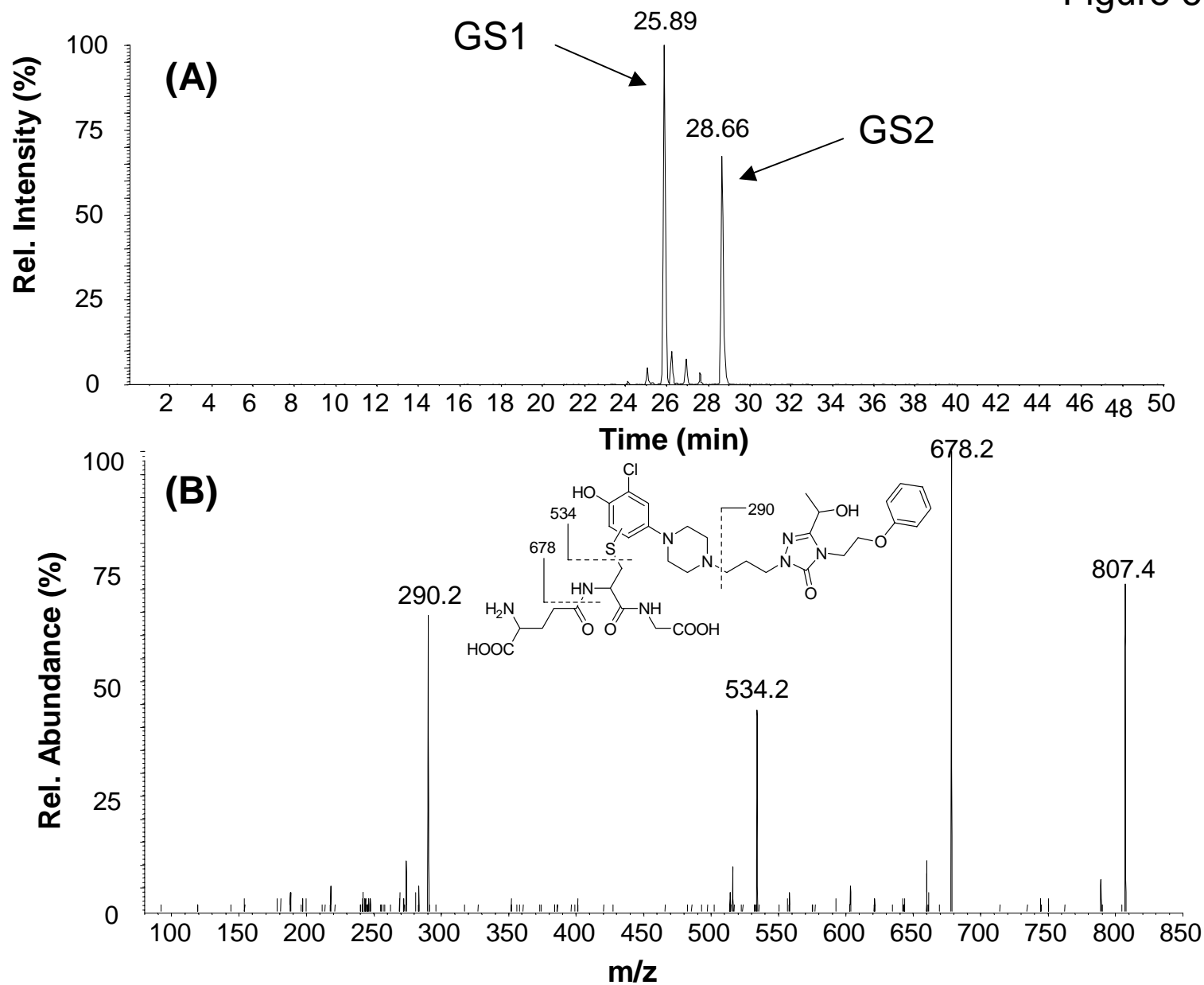


Figure 7

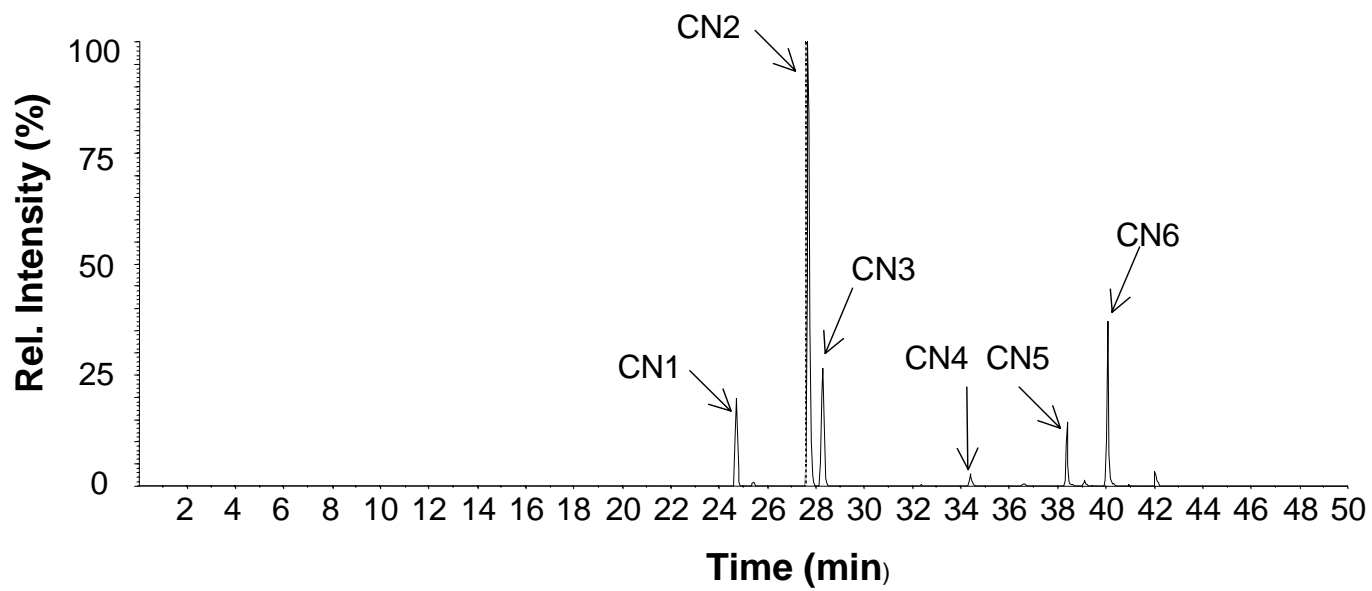


Figure 8

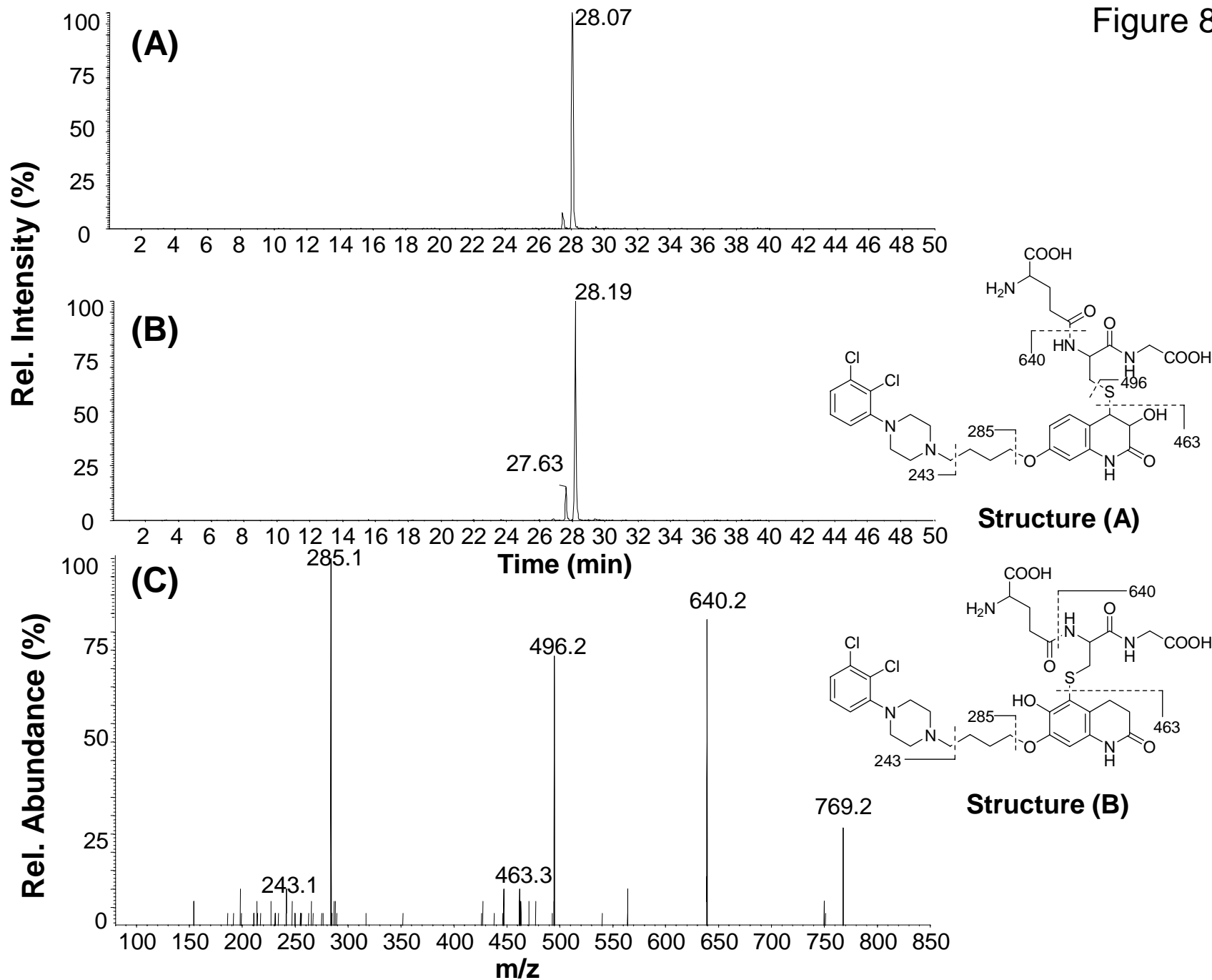


Figure 9

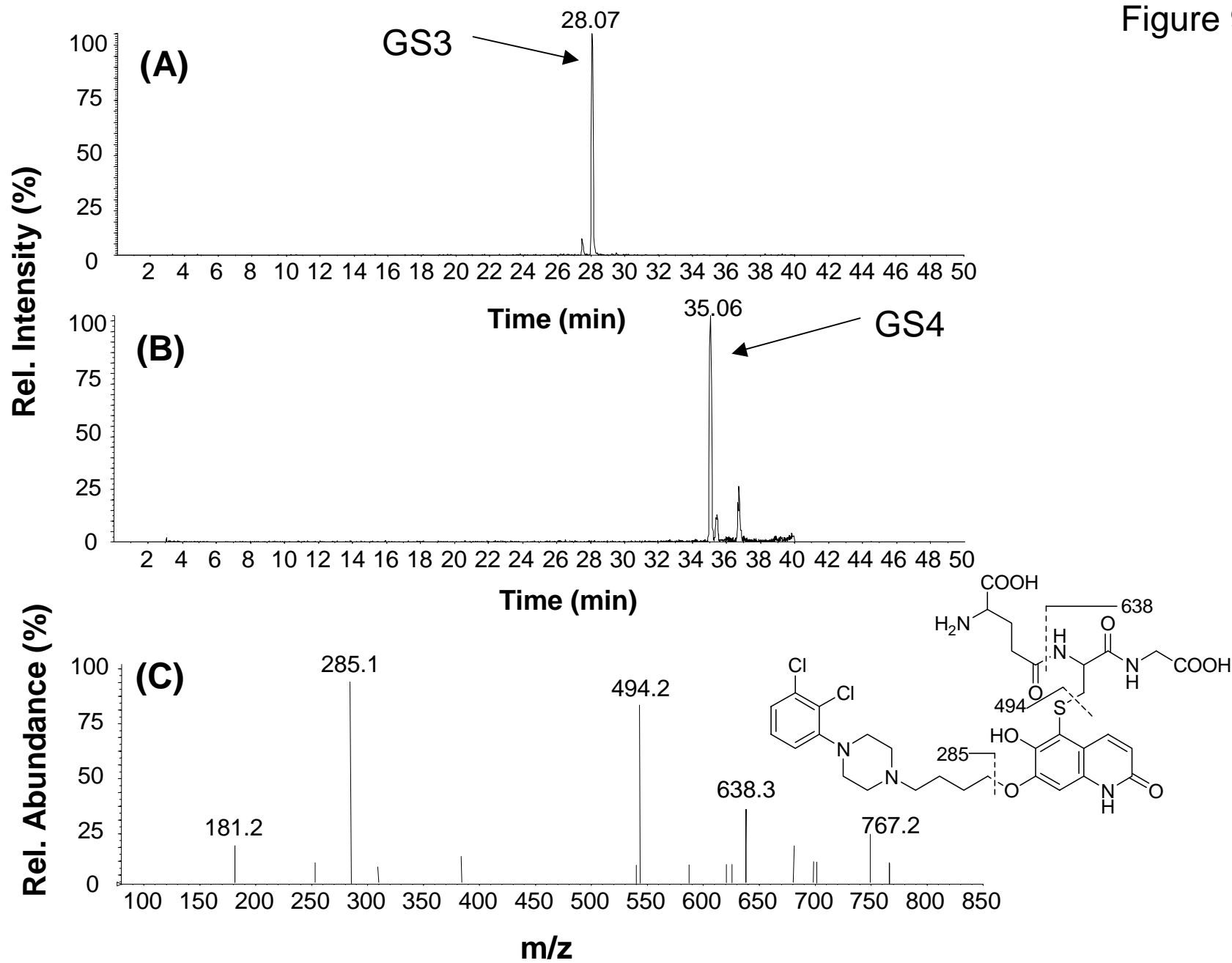


Figure 10

